JOURNAL OF GEOPHYSICAL RESEARCH, VOL. 113, D16112, doi:10.1029/2008JD009864, 2008

Click Here for Full Article

# Annual amphidromes observed in the atmosphere with remote sensing data

Caiyun Zhang,[1,2] Ge Chen,[2] and Fang Qiu[1]

Received 24 January 2008; revised 30 May 2008; accepted 11 June 2008; published 26 August 2008.

[1] Annual cycle, one of the principle modes in the variability of the air-sea system, can be analyzed using tide analysis tools for extending the concept of oceanic tidal amphidromes to the atmosphere. In this paper, the annual phase-amplitude characteristics of two variables, sea-level pressure (SLP) and precipitation, were investigated to explore the annual atmospheric amphidromes on a global scale. For SLP, around a dozen annual amphidromic points were successfully identified. These points are distinguished by large-scale rotary phase propagations around them. For global precipitation, we identified a substantial amount of annual rainfall amphidromic points, with many of them appearing as pairs close to each other and less developed. Further examinations illustrate that these rainfall amphidromes tend to occur in narrow bands or small regions with low annual amplitudes and phase structures opposite to their surroundings. This suggests that precipitation amphidromes tend to appear as quasi-amphidromic lines or quasi-amphidromic zones. The occurrence of El Niño/La Niña events does not affect the formation and stability of SLP and precipitation amphidromes, although it can modify the annual variations in terms of amplitude and phase changes.

**Citation:** Zhang, C., G. Chen, and F. Qiu (2008), Annual amphidromes observed in the atmosphere with remote sensing data, *J. Geophys. Res.*, *113*, D16112, doi:10.1029/2008JD009864.

## 1. Introduction

[2] As a scientific term describing the oceanic tidal system, an ''amphidrome'' normally refers to an oceanic point where there is almost zero tidal amplitude and undetermined phase because of the canceling of tidal waves. There are about a dozen well-defined tidal amphidromes identified for diurnal and semidiurnal tides, which constitute a fundamental feature in the global ocean system [*Cartwright*, 2001].

[3] It is widely understood that many geophysical variables in the air-sea system exhibit significant annual variability because of the strong seasonality caused by solar irradiance. The annual cycle in the variability of the air-sea system, in a sense, behaves just like the ebbs and flows of the tidal system. Therefore amphidromes of such kind may also be identified in some key oceanic and atmospheric parameters. In *Chen and Quartly* [2005] (abbreviated as CQ2005 hereafter) successfully identified annual oceanic amphidromes in two variables, sea level anomaly (SLA) and sea surface temperature (SST). Their findings suggest that amphidromes are not only tidal phenomenon, but also are common features of the global oceans. Further studies illustrated that annual oceanic amphidromes exist not only on a global scale, but also in regional seas, such as those identified in the South China Sea (SCS) [*Zhang et al.*, 2006]. These interesting findings lead to the speculation that annual amphidromes might also exist in the atmosphere, where annual variability is also significant. In this paper, we focus on identifying annual atmospheric amphidromes based on annual phase and amplitude diagrams of sea-level pressure (SLP) and precipitation, which agree with previous studies indicating that the phase-amplitude features of key parameters in the air-sea system can reveal new aspects of climate variations [e.g., *Wang et al.*, 2000; *Chen and Lin*, 2005].

[4] To examine the stability of amphidromes in the atmosphere, we explored the impacts of El Niño/La Niña and warm/cold regimes of decadal variation on the annual phase-amplitude characteristics. It is well understood that the low-frequency variability of the air-sea system is composed of several systematic modes ranging from seasonal to decadal time scales. Among them, the semiannual cycle, the annual cycle, the El Niño-Southern Oscillation (ENSO) [*Philander*, 1983] and the Pacific Decadal Oscillation (PDO) [*Mantua et al.*, 1997] are of major dominance. The characteristics and physical dynamics of each mode have been extensively studied during the past decades; however, the interrelationships between these low-frequency modes and the manner in which they interact with one another are not entirely clear [e.g., *McPhaden*, 1999]. As far as the relationship between ENSO and the annual cycle is concerned, previous studies illustrate that the ENSO signal

[1]Program in Geospatial Information Sciences, University of Texas at Dallas, Richardson, Texas, USA.
[2]Ocean Remote Sensing Institute, Ocean University of China, Qingdao, China.

Copyright 2008 by the American Geophysical Union.
0148-0227/08/2008JD009864$09.00

exhibits a preferred phasing with the annual cycle [e.g., *Rasmusson and Carpenter*, 1982]. ENSO can also modify the annual cycle by changing the annual amplitude and shifting the annual phase of some variables [*Gu and Philander*, 1995; *Chen and Lin*, 2005]. The PDO has received much attention in the world and has been described as a long-lived El Niño-like pattern of Pacific climate variability. Several studies document the relationship between PDO and ENSO [*Mantua et al.*, 1997; *Zhang et al.*, 1997; *Newman et al.*, 2003], but there is still considerable uncertainty on whether the PDO is truly independent of the leading ENSO mode of the tropical Pacific. Investigations about the relationship between PDO and the annual cycle are very limited and little has been written about it. Examining impact of these two quasi-periodic oscillations on the annual SLP cycle and precipitation cycle in terms of amplitude change and phase shift can help us understand the interrelationship between these climate modes and the stability of the identified amphidromes.

[5] The identification of amphidromes in the atmosphere is important. Ideally, amphidromes are free of the interference from strong annual cycle signals and would therefore provide ideal locations for gauge and buoy deployment, achieving effective and efficient observations of other climate modes at seasonal to decadal time scales. This is important because these climate modes usually affect many natural and societal activities over the globe. In addition, these atmospheric amphidromes can be used as benchmarks for validating or comparing numerical models. Therefore this paper will contribute to the understanding of annual variabilities in the air-sea system in general and knowledge of atmospheric amphidromes in particular.

## 2. Data and Processing

### 2.1. Extended Reconstructed SLP Data

[6] The SLP data used in this study was derived from the extended reconstructed SLP (ERSLP) product compiled by *Smith and Reynolds* [2004]. This monthly ERSLP product at $2^\circ \times 2^\circ$ grid was constructed using the most recently available Comprehensive Ocean-Atmosphere Data Set (COADS) SLP data and improved statistical methods that allow stable reconstruction of SLP using sparse data. The advantages of this product can be summarized as: (1) it has a long-duration spanning from 1854 to 1997 at monthly level; and (2) it has superior quality because of the assimilation of satellite observations starting in 1979. The long duration allows for impacts of the decadal variation on annual variation of SLP to be investigated and the superior quality can make the identification of annual amphidromes more convincing.

### 2.2. Global Precipitation Climatology Project (GPCP) Rainfall Data

[7] The GPCP precipitation product was derived from World Data Center for Meteorology of National Oceanic and Atmospheric Administration (NOAA). GPCP version 2 provides monthly, global $2.5 \times 2.5$ degree grids of rainfall products spanning from January 1979 to the delayed present. It combines rainfall information from microwave estimates based on Special Sensor Microwave/Image (SSM/I) data, the infrared precipitation estimates obtained primarily from geostationary satellites operated by the United States, Europe, and Japan, and secondarily from polar-orbiting satellites, as well as the gauge data assembled. GPCP has compensated for the weaknesses of each individual precipitation estimates and has developed an improved blending scheme to merge these multi-source precipitation products into one global product. Detailed description of this product can be found in the work of *Adler et al.* [2003].

### 2.3. Data Processing

[8] To extract annual phase-amplitude information, harmonic analysis was employed. Harmonic analysis is a traditional but very useful method in climate study. It assumes that a climate signal can be decomposed into a series of harmonic waves with regular periods such that:

$$S(t) = S_0 + \sum_{k=1}^{N} \left( \cos\left(\frac{2k\pi}{T} t\right) + \sin\left(\frac{2k\pi}{T} t\right) \right) \quad (1)$$

where $S(t)$ is the observed scalar, $S_0$ is the climatology mean, $N$ and $T$ are wave number and period, respectively. It can also be written as:

$$S(t) = S_0 + \sum_{n=1}^{N} A_n \cos\left(\frac{2\pi}{T_n} t + \varphi_n\right) \quad (2)$$

where $A_n$ and $\varphi_n$ denote the amplitude and phase lag of each harmonic wave. In this study, we set $T = 12$ months and $N = 2$. The first harmonic wave was used to produce the annual phase and amplitude diagrams. During the harmonic analysis, two coefficients were estimated for each harmonic wave and used to calculate the harmonic amplitude and phase. The phase refers to the calendar month during which the annual SLP or precipitation peaks. For visualization, the amplitude plot was created by using a smoothed contour map and the phase plot was created by a classified post map that was not smoothed. During the whole calculation, no smoothing steps were performed.

## 3. Annual SLP Amphidromes

### 3.1. Annual Phase and Amplitude Diagrams

[9] According to *Hsu and Wallace* [1976, abbreviated as HW1976 hereafter], many early efforts [e.g., *Hann and Süring*, 1939; *van Loon*, 1972] were made to improve our understanding of annual SLP variations on a global scale. However, these studies were conducted based on pressure data derived from a few station measurements available at the time. In the past decades, tremendous advancements have been made both in SLP measurement techniques and data processing capability, especially with the inclusion of observations from remote sensing techniques. These advancements make better SLP data products available with higher spatial resolutions, superior quality and longer duration on a global scale. To reexamine the annual variation of SLP using these improved data products, we compiled 21-year data out of the ERSLP product spanning January 1977 to December 1997. The harmonic analysis was then applied to the twelve calendar months data at each grid, which were derived by averaging data for each month over all the years during this period. The result is shown in Figure 1.

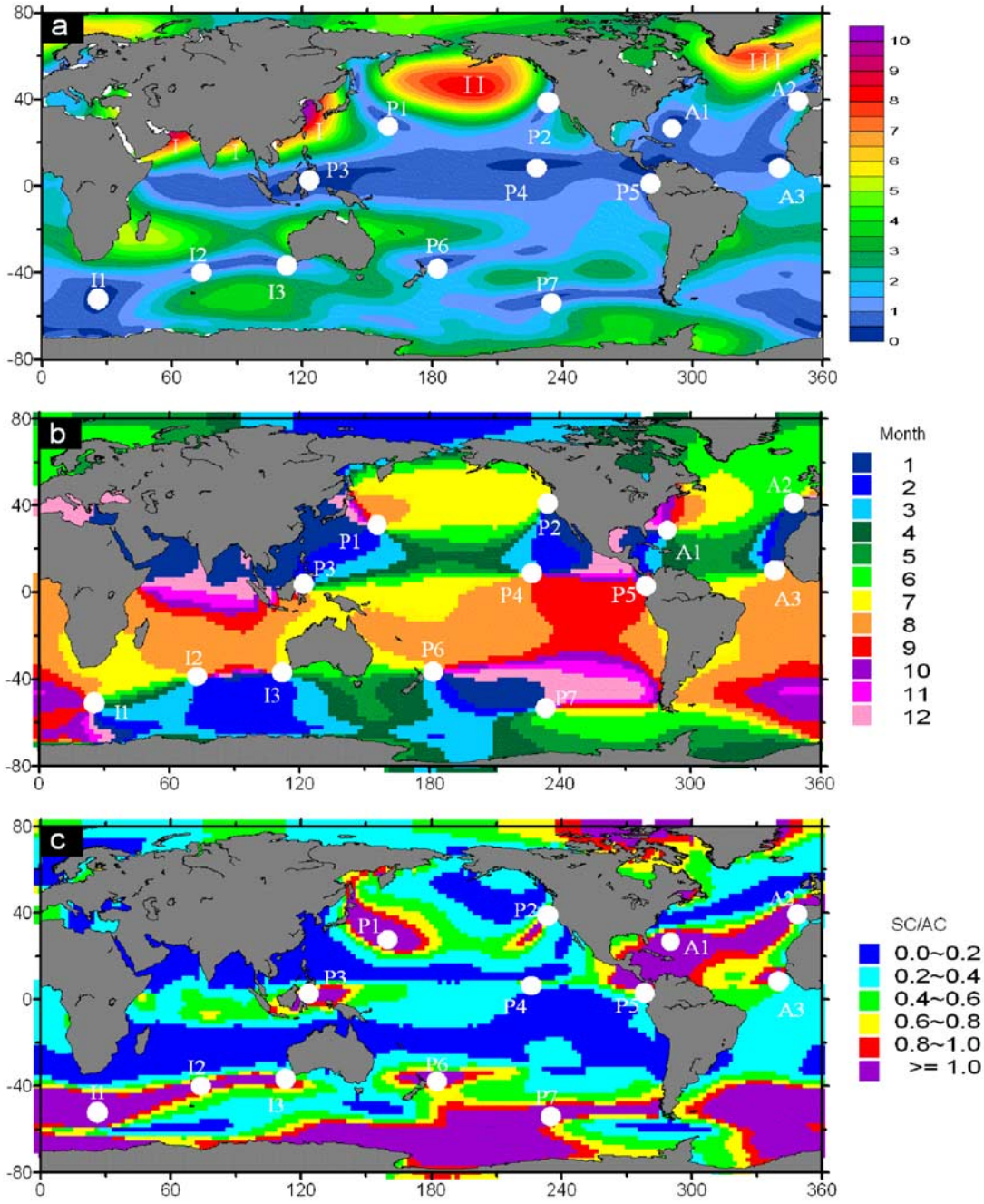


**Figure 1.** Maps of SLP for (a) annual amplitude (unit: mb), (b) annual phase, and (c) ratio of semiannual cycle to annual cycle amplitude. The white dots denote the identified annual SLP amphidromic points.

[10] The annual amplitude pattern of SLP is characterized by three high-amplitude SLP zones (in red, labeled I, II, and III) in the Northern Hemisphere (NH), small amplitudes in the tropical areas (in blue), and moderate amplitudes (in green) in the Southern Hemisphere (SH) (Figure 1a). In the NH, high-amplitude zone I, extending from the Arabian Sea to the Sea of Japan along the coast of the Asian continent, is closely associated with the Asian monsoon, whereas zones II and III observed in the north-central Pacific and Atlantic, respectively, may be related to the landmass distribution and mass transport between the polar cap and the midlatitudes [*Lorenz*, 1951]. Low-amplitude areas detected over the tropical oceans geographically coincide with the small seasonality identified for other key variables, such as water vapor [see Figure 6b of *Chen*, 2004] and SST [see Figure 2a of *Zhang and Chen*, 2007]. This may be due to the combination of strong tropical ENSO signal and the semi-annual cycle of solar irradiance resulting from the crossing of the Sun over the equator twice a year, which significantly weakens the annual cycle in this region. The moderate

**Table 1.** Geographical Location of Annual SLP Amphidromic Points

| Ocean | Amphidrome | Location |
|---|---|---|
| Pacific Ocean | P1 | (160°E, 29°N) |
| | P2 | (233°E, 39°N) |
| | P3 | (123°E, 3°N) |
| | P4 | (228°E, 8°N) |
| | P5 | (280°E, 2°N) |
| | P6 | (183°E, 38°S) |
| | P7 | (235°E, 55°S) |
| Indian Ocean | I1 | (26°E, 52°S) |
| | I2 | (74°E, 40°S) |
| | I3 | (113°E, 36°S) |
| Atlantic Ocean | A1 | (290°E, 26°N) |
| | A2 | (349°E, 40°N) |
| | A3 | (340°E, 8°N) |

amplitudes in the SH are related to landmass distributions and the pronounced semiannual oscillation over middle and high latitudes [*van Loon*, 1967].

[11] The global annual SLP phase is shown in a classified post map (Figure 1b). The phase refers to the calendar month during which the annual SLP peaks. This map reveals detailed information about global SLP seasonality. The annual SLP phase can be divided into five zonal bands from the North Polar Region to South Polar Region. An interesting observation is that each band consecutively reaches its annual SLP maximum in either the first half of the year or the second half of the year following an alternating pattern. HW1976 pointed out that the North Polar Region tends to have a maximum in boreal spring, while a majority of subtropical and midlatitude oceans usually have maxima in boreal summer. On the contrary, in the SH, only a minority of subtropical oceans tends to reach maximum in boreal winter. In the tropical Pacific and Atlantic Oceans, SLP peaks conversely in time between the two hemispheres. The Indian Ocean follows a SLP pattern that propagates from the SH to the NH. This is related to the Asian monsoon that drives the cross-equatorial flow in the Indian Ocean.

[12] Examining the relative importance of annual cycle and semiannual cycle is very helpful for identifying amphidromic points. This can be quantified by estimating the ratio of two harmonic amplitudes at each grid, as illustrated in Figure 1c. The spatial ratio map reveals that the relative importance of two periodic signals is inhomogeneous over the global oceans. A majority of oceans have strong annual cycle with a ratio less than 1.0 and a minority of oceans has strong semiannual cycle (in purple). The area-averaged ratio for the global ocean is roughly estimated to be 0.47, suggesting that the magnitude of the annual cycle is more prominent than the magnitude of the semiannual cycle. Ratio plot is also related to the amphidromic issue to be discussed below.

### 3.2. Annual SLP Amphidromes

[13] Recalling that an amphidrome is characterized by its undetermined phase and almost zero amplitude, we identify thirteen nodal points, P1, P2, P3, P4, P5, P6, P7, I1, I2, I3, A1, A2, and A3 in the annual SLP phase pattern in Figure 1b. P1 is a distinct annual SLP amphidromic point with a cyclonic phase propagation around it. P2 is a nodal point located to the west of North America with a partial sequential of a year. The rest of the rotary system around P2 is presumably hidden by land. Unfortunately, we cannot obtain any information over land because the ERSLP product only covers ocean data. This could be tested in the future with land SLP data. P3, P4 and P5 are situated over the equatorial Pacific from west to east. P6 and P7 constitute a pair of amphidromes, with opposite rotations and positioned in the central South Pacific. In the Indian Ocean, we identified three amphidromic points, I1, I2, and I3, which demonstrate a similar pattern as P3, P4, and P5. In the Atlantic Ocean, we identified three nodal points. A1 is a well-defined amphidrome with a cyclonic rotation in the Atlantic Ocean. It is related to the Pacific amphidrome P5 by sharing some of its co-phase lines. A2 and A3 appear in pair and demonstrate partial sequential rotary phase features as P2. These thirteen amphidromes are well separated geographically, but they are associated with each other by sharing some co-phase lines with their neighbors, which present a striking structure in annual SLP phase.

[14] To further examine the existence of SLP amphidromes, we projected their geographic locations (see Table 1) on the related annual amplitude plot in Figure 1a and the ratio plot in Figure 1c. These amphidromes are indeed located in the regions with low annual amplitudes. All of them are also located in regions where semiannual cycle is stronger than the annual cycle with the exception of P4. This is a better indicator for the existence of amphidromes than absolute annual amplitude because these locations reflect additional information about the semiannual component. By combining the annual phase and amplitude diagrams, we can define an annual SLP amphidrome as an atmospheric point at which the annual SLP amplitude is less than 1mb and the phase is undetermined.

### 3.3. Impacts of El Niño/La Niña

[15] In this section, we examined the impacts of El Niño/La Niña on annual phase-amplitude features and the stability of identified annual SLP amphidromes.

[16] As we know that the ENSO variability has two extremes, taking one form in El Niño and another in La Niña. National Centers for Environmental Prediction (NCEP) Climate Prediction Center (CPC) of NOAA compiled a list of cold (La Niña) and warm (El Niño) episodes by using reanalyzed SST to provide a season-by-season breakdown of conditions in the tropical Pacific (more information available online at http://www.cpc.ncep.noaa.gov/products/analysis_monitoring/ensostuff/ensoyears.shtml). We considered a particular year as an El Niño (La Niña) year if two or more seasons were designated as warm (cold) events with moderate or strong strength. For the purpose of examining impacts, we divided the 21-year period SLP data into two groups, one for the El Niño years (1977, 1982, 1987, 1991, 1992, 1994, and 1997) and the other for La Niña years (1985 and 1988). This asymmetric sampling scheme, seven El Niño events verse two La Niña events, may affect the resulting patterns. Harmonic analysis was then performed separately for the averaged El Niño and La Niña composites to derive the annual phase-amplitude diagrams, as shown in Figure 2.

[17] From the geographical distribution of annual SLP amplitude for El Niño years (Figure 2a) and La Niña years

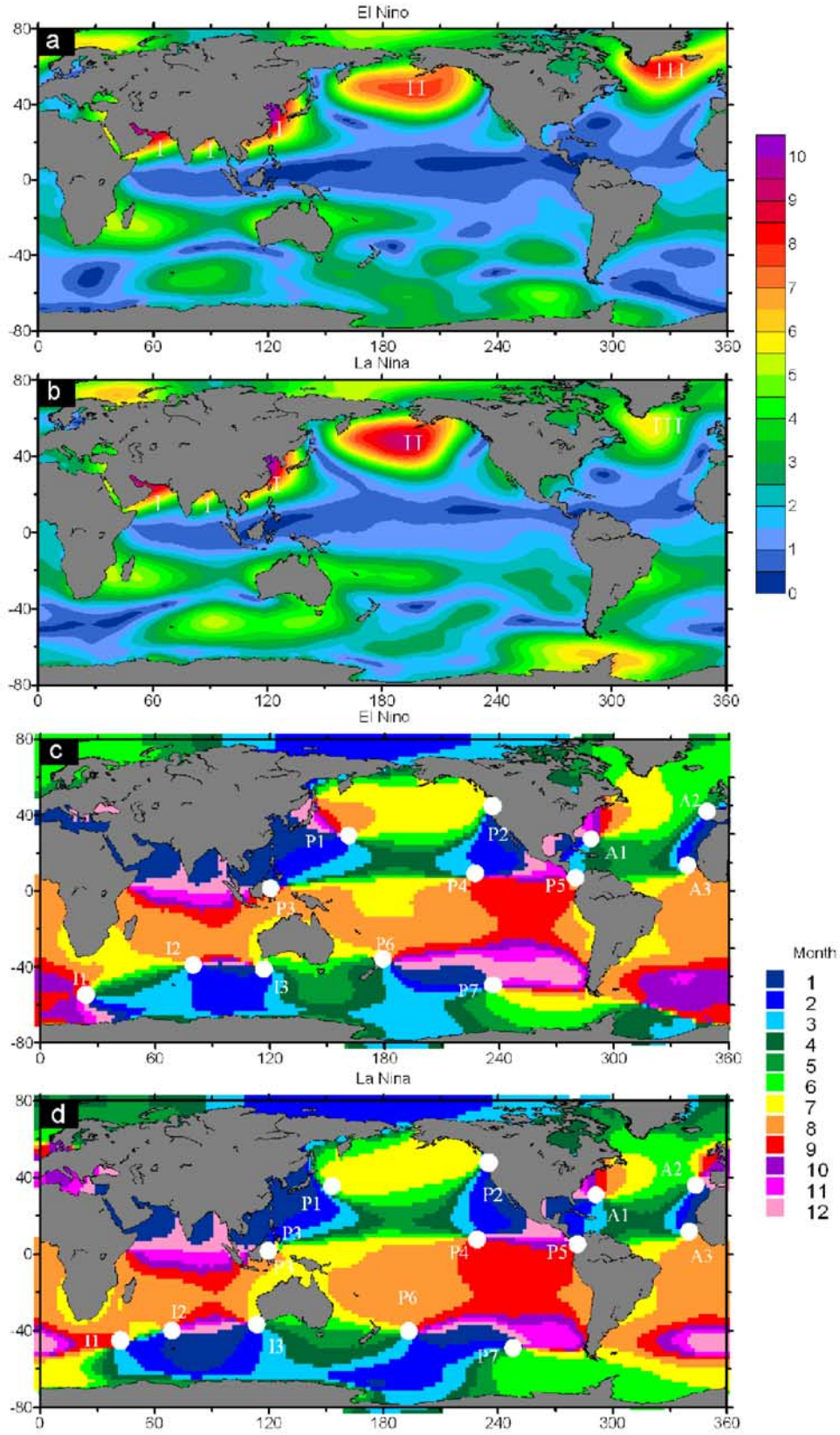


**Figure 2.** Maps of annual amplitude of SLP for (a) El Niño years, (b) La Niña years, and annual SLP phase for (c) El Niño years and (d) La Niña years. The white dots denote the identified annual SLP amphidromic points.

(Figure 2b) years, we can see that the ENSO has an impact on the annual SLP variation by changing its annual amplitude. This was particularly evident because of the shift of the center of the location and the modification of the amplitude strength for the high-amplitude zone II and zone III in the NH. The tropical low-amplitude zonal band was enhanced/weakened by shrinking/extending its meridional width during El Niño/La Niña years. In the SH, notable changes over moderate amplitude zones were observed. The global mean annual amplitude was decreased/increased about 0.5mb during El Niño/La Niña events, which agrees with results derived for the oceanic water vapor variable [*Chen and Lin*, 2005].

[18] Similar behaviors can also be found in the annual phase patterns as a result of the phase-amplitude coupling. The annual phase patterns under El Niño and La Niña years are presented in Figures 2c and 2d respectively. A striking feature of these two maps is the systematic phase shift between the two ENSO modes in terms of geographical location. Specifically, the August–December peak pattern located north of the amphidromic point P1 disappeared for the La Niña years and a minority of oceans in the midlatitude of North Atlantic advanced a month in reaching their maxima. The rotated phase structure hidden by land during the El Niño years becomes well developed around A2 in La Niña years. In the SH, some notable features can also be found. The South Pacific August pattern was zonally stretched and a minority of oceans South of Africa delayed a month in reaching their maxima in La Niña years compared to the El Niño years.

[19] As supported by the above arguments, the ENSO signal can change the annual variations of SLP by modifying the phase and amplitude. However, the thirteen amphidromic points can still be identified in the phase patterns of both El Niño and La Niña years. The large-scale rotary phase structures around these points are evident. The ENSO cycle does not have a significant impact on the geographical location of most of the nodal points, although their surrounding phase structures were slightly modified by these two events. Large location displacement was observed for I1, which migrated northeasterly in La Niña years. A2 became clearer with the appearance of a full annual sequential pattern around it (Figure 2d).

### 3.4. Impacts of Decadal Variation

[20] It is also important to examine the impacts of warm/cold episodes of PDO on annual phase-amplitude features and the stability of annual SLP amphidromes. According to *Mantua et al.* [1997], only two full PDO cycles were identified in the past century. Cool phase prevailed from 1890–1924 and again from 1947–1976, while warm PDO regimes dominated from 1925–1946 and from 1977 through (at least) the mid-1990s. The ERSLP data covering the period from 1854 to 1997 provides an opportunity to assess the impact of PDO on the annual cycle in terms of amplitude changes and phase shifts. We divided the extended data into two subsets, a cool phase (1890–1924 and 1947–1976) and a warm phase (1925–1946 and 1977–1997). Harmonic analysis was then performed on the averaged cool and warm composites. The results are shown in Figure 3.

[21] From the geographical distribution of annual amplitude for warm (Figure 3a) and cool (Figure 3b) PDO variation regimes, we see that the annual amplitude of SLP for the warm phase was different from that for the cold phase. Notable features can be observed over zone II and zone III. The annual variability was weakened for zone II during cool phase compared with that of the warm phase. This is different from the impact of ENSO on this region in that La Niña enhanced the annual amplitude (Figure 2a). However, weakened annual variation was observed over zone III under the cool events of both ENSO and PDO. Some slight differences can also be found between the two regimes, such as the small displacement of the centroid locations for some moderate amplitude zones in the SH. We did not find distinctive differences for the eastern tropical Pacific although both ENSO and PDO are significant in this region.

[22] The phase plots for warm and cold PDO regimes are shown in Figures 3c and 3d respectively. Notable phase shifts were found in the midlatitude of NH where significant amplitude changes were observed. For the warm phase (Figure 3c), the July pattern was stretched in the North Pacific compared to that of the cold phase (Figure 3d). However, an opposite shift was found in the North Atlantic where the July pattern was shrunk for the warm phase. A noticeable phase shift was also observed in the Mediterranean Sea where certain areas reached their annual maximum a month earlier for the cool phase than for the warm phase.

[23] From the annual phase patterns for the warm and cool events, thirteen amphidromes can still be observed (Figures 3c and 3d), and their geographical locations are stable (within 5°) under both modes. Although the PDO is an ENSO-like signal, the PDO and ENSO have different impacts on the annual SLP variations. However, neither PDO nor ENSO has influence on the formation of these amphidromic points and their observed geographical locations.

## 4. Annual Precipitation Amphidromes

### 4.1. Annual Phase and Amplitude Diagrams

[24] Following the successful identification of annual amphidromes for SLP, we were inspired to investigate other atmospheric variables to see if we could also detect similar features. Precipitation was selected for this purpose because of its extensive usage in climate studies and its key role in climate system. We compiled 26-year precipitation data spanning January 1980 through December 2005 from GPCP data. Harmonic analysis was then performed. The resulting annual phase and amplitude diagrams are shown in Figure 4.

[25] The spatial pattern of annual precipitation amplitude is characterized by large amplitudes over tropical oceans and small amplitudes over middle and high latitudes in both hemispheres (Figure 4a). Unlike its corresponding pattern for SLP (Figure 1a), the precipitation cycle is more symmetric between the NH and SH. A salient feature of this distribution is that high amplitudes are closely tied to global monsoon domains defined by precipitation, and they tend to reside on each side of the equatorial perennial rainfall regions [see Figure 1a of *Wang and Ding*, 2006]. This suggests that global monsoon domains based on precipitation can be derived by the annual amplitude distributions.

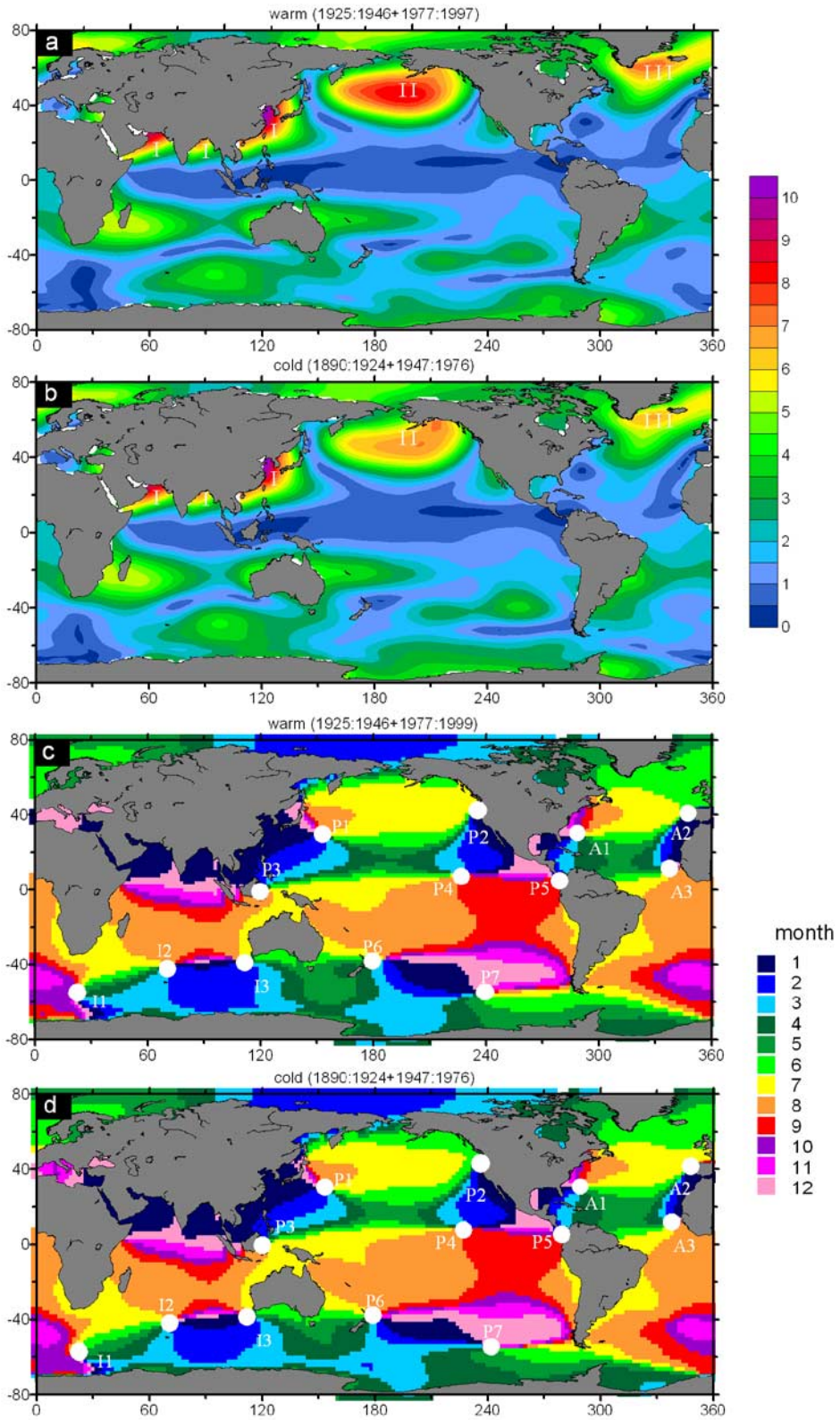


**Figure 3.** Maps of annual amplitude of SLP for (a) warm phase, (b) cold phase, and annual SLP phase for (c) warm phase and (d) cold phase of decadal variability. The white dots denote the identified annual SLP amphidromic points.

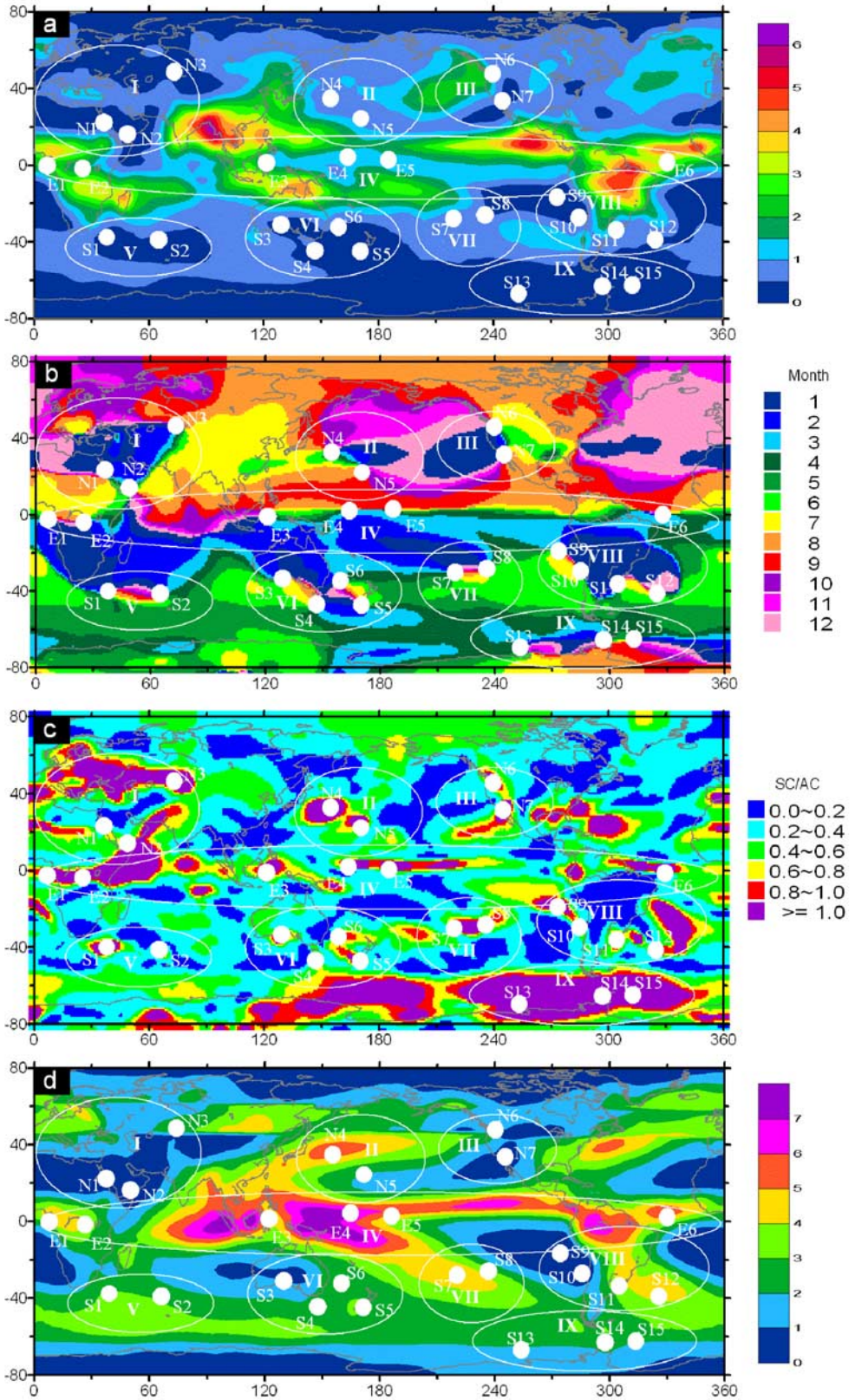


**Figure 4.** Maps of precipitation for (a) annual amplitude (unit: mm/day), (b) annual phase, (c) ratio of semiannual cycle to annual cycle amplitude, and (d) climatology (unit: mm/day) during 1980–2005. The white dots denote the identified amphidromic points. Eight quasi-amphidromic zones and one quasi-amphidromic line are also highlighted.

The amplitude pattern differs from the climatological pattern of rainfall (Figure 4d), which is characterized by the tropical rain maximum in the eastern Indian Ocean and western Pacific, rain belt in the equatorial area, several desert zones in the midlatitudes, and dry regions in the high latitudes.

[26] As far as the phase distribution is concerned (Figure 4b), a pattern of anticorrelation in rainfall seasonality is observed between the two hemispheres with the equator serving roughly as a dividing line. A majority of regions in the SH and NH reach their maxima in the first and second half of the year respectively. The SH can be further divided into two seasonal regimes, the tropical regime with maximum rainfall from January to March and the extratropical regime with maximum rainfall in April and June.

### 4.2. Annual Rainfall Amphidromes

[27] A large number of amphidromic points are observed for annual rainfall phase distributions. These points, however, are different from those observed for SLP (Figure 1), as well as those for SLA and SST [see Figures 1 and 2 of *Chen and Quartly*, 2005] in the following three aspects. First, most of the annual phase rotary scale surrounding the amphidromic points is smaller, such as that of N1/N2, E1/E2, and S1/S2. Second, many of the points appear as pairs and irregular in nature. Third, there are more amphidromes identified for precipitation than for SLP, SLA and SST. An interesting question then arises: why are annual rainfall amphidromes so different from those of other variables?

[28] To answer this question, we first projected all the nodal points on the corresponding amplitude diagram in Figure 4a. These amphidromes are located in regions where annual rainfall amplitudes are very small. By combining the annual phase and amplitude diagrams, we can define an annual rainfall amphidrome that is a point where rainfall amplitude is less than 1mm and has rotary phase propagation around it or the phase by itself is undetermined. Further observations from the rainfall phase and amplitude diagrams illustrate that these amphidromic points are mainly distributed in nine areas, highlighted by the white ellipses in Figure 4. Among these nine areas, eight have opposite phase structures with a small spatial scale compared with the major phase regions surrounding them, and one (area IV) is a transitional band between two hemispheres. We further projected these nine regions with their corresponding amphidromic points over the rainfall climatological map (Figure 4d). We found that some points were located in high precipitation areas (such as region II and VI), some in very low precipitation areas (such as region I and III), and others in moderate precipitation areas. On the basis of the characteristics of rainfall amphidromes, we extend the scientific term of amphidrome originally used in the ocean tidal system. Amphidrome includes (1) a point that small amplitude and undetermined phase are observed with large-scale rotary phase structure formed around it, such as those observed in SLP, SLA, SST and the global tidal system; (2) a narrow band, termed quasi-amphidromic line, where small amplitude is observed with well-defined or ill-defined amphidromic points developed along it, such as region IV in Figure 4; and (3) a small region, termed quasi-amphidromic zone, where out-of-phase structure and small amplitude compared to its surroundings are observed. Amphidromic points can be developed along the boundary of these quasi-amphidromic zones, such as those in the highlighted areas except for area IV. With the extended definition of amphidrome, we are able to identify eight quasi-amphidromic zones and one quasi-amphidromic line in the global annual variation of precipitation.

[29] The ratio of semiannual and annual harmonic amplitudes is presented in Figure 4c with rainfall amphidromic points included. We can see that these points are located in regions where the semiannual component is more significant than the annual component, suggesting the formation of annual rainfall amphidromes may be related to the semiannual component.

### 4.3. Impacts of El Niño/La Niña

[30] Following similar steps for examining annual SLP amphidromes under El Niño and La Niña modes, we divided the 26-year precipitation data into two subsets, one for El Niño years (1982, 1987, 1991, 1992, 1994, 1997 and 2004), and one for La Niña years (1985, 1988, 1999 and 2000). We also applied harmonic analysis to the averaged El Niño and La Niña composites. The results are shown in Figure 5.

[31] The El Niño and La Niña also affect the annual variability of rainfall by changing its amplitude and phase structures. This is particularly evident over the seasonally dynamical zones, in that their intensities and their centroid locations were shifted from El Niño to La Niña (Figures 5a and 5b). Notable phase shifts can also be observed over areas II and III, where the January pattern connected during La Niña years and separated during El Niño years. Another rotary phase structure can be observed in the upper left of area I for La Niña mode (Figure 5d). The phase structures around E4 and E5 underwent dramatic changes from one mode to another (Figures 5c and 5d).

[32] Both the annual phase and the annual amplitude of rainfall were modified by El Niño/La Niña. However, the eight quasi-amphidromic zones, the equatorial quasi-amphidromic line, and amphidromic points still can be identified with small shifts in the location of some amphidromic points. The annual phase-amplitude diagram was also derived using the simultaneous estimates of precipitation from CPC Merged Analysis of Precipitation (CMAP) data set [*Xie and Arkin*, 1997]. In general, the result (not shown) is consistent with the amphidromic characteristics presented in the GPCP data set. However, not all the amphidromic points are observed. A few are missing or becoming unclear, such as N2, N3, N4, N5, S9 and S10. This is attributed to differences between the two data sets and their relatively lower spatial resolution. The rainfall amphidromic points developed along a quasi-amphidromic line or within a quasi-amphidromic zone appear less stable in both location and formation. It is also noted that some rainfall amphidromic points are located in very low precipitation regions (N1/N2, N6/N7, and S9/S10), which might critically affect the statistical results presented here. However, if these points really exist, they should be observed along a quasi-amphidromic line or within a quasi-amphidromic zone. We cannot examine the impact of decadal variation on annual variations of rainfall because of the limited duration of the

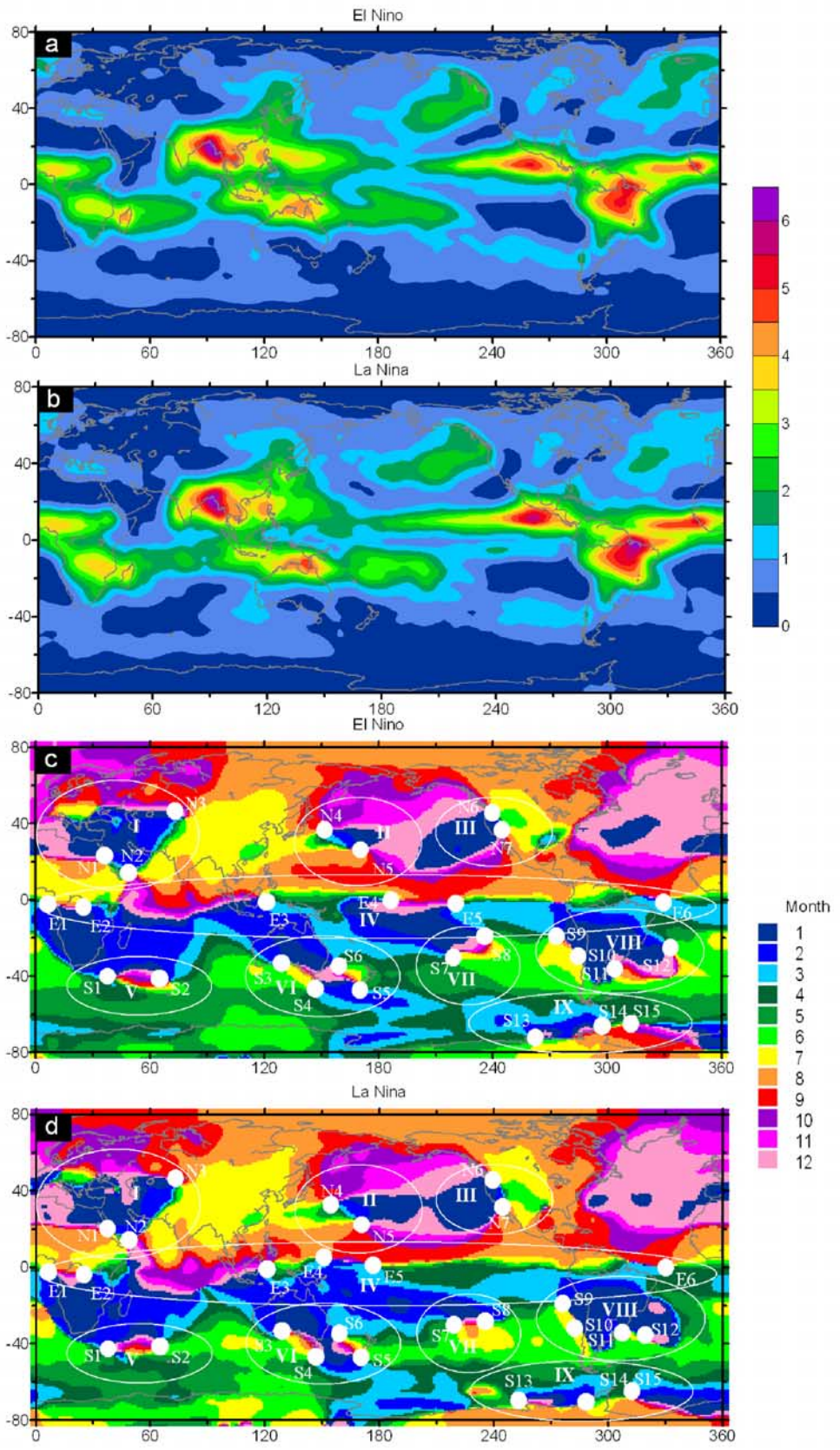


**Figure 5.** Maps of annual amplitude of precipitation for (a) El Niño years, (b) La Niña years, and annual precipitation phase for (c) El Niño years and (d) La Niña years. The white dots denote the amphidromic points. Eight quasi-amphidromic zones and one quasi-amphidromic line are also highlighted.

data. This can hopefully be tested using outputs from numerical models in the future.

## 5. Summary and Discussions

[33] The global feature of annual amphidromes in the atmosphere is revealed by examining the characteristics of annual SLP and precipitation phase and amplitude diagrams. The main findings are summarized as follows. First, thirteen well defined annual SLP amphidromic points are identified in the global atmosphere. These points are characterized by their small annual SLP amplitudes and the large-scale rotary phase propagations around them. Second, substantial amounts of annual precipitation amphidromes are observed. Unlike those identified for SLP, SLA and SST, these rainfall amphidromes are better characterized by quasi-amphidromic lines or quasi-amphidromic zones. Annual precipitation amphidromic points are usually found along a quasi-amphidromic line or within a quasi-amphidromic zone. They tend to appear as pairs close to each other, are irregular in nature, and have small-scale rotary phase propagations around them. Some of the rainfall amphidromic points are not stable, especially those observed in very low precipitation areas. In the future, reliability of these points needs to be examined by using data sets with higher spatial resolution and superior quality. Third, El Niño/La Niña events have impact on the annual variations of SLP and precipitation by changing their annual amplitudes and shifting their annual phases; however, they do not affect the formation and stability of these amphidromes. The identification of amphidromes in the atmosphere has several important implications. First, amphidromes are theoretically free of the interference from strong annual signals and therefore are ideal locations for gauge and buoy deployment in order to achieve effective and efficient observations of other climate variation modes. Second, these amphidromes can be used as benchmarks for validation and comparison for numerical models. Third, amphidromes provide an alternative research perspective to the understanding of annual variations in the air-sea system, particularly with the extension of oceanic tidal amphidromes into the atmosphere. Finally, the phase and amplitude diagrams provide an insight into how annual variations at different locations link to each other. The diagrams display the phase propagation and associated singular points, which are helpful to the physical interpretation of the annual variations of the two variables.

[34] Different from tidal amphidromic points that are supported by the mature Kelvin wave theory, annual amphidromes are newly discovered features by CQ2005 and further studied by *Zhang et al.* [2006] and *Zhang and Chen* [2007]. The physical dynamics of annual amphidromes may be different for different oceanic and atmospheric variables. They are likely to differ at different locations even for the same variable. We made some efforts in explaining the formation of annual sea level amphidromes in the SCS and for annual SST amphidromes in global oceans using empirical orthogonal function (EOF) analysis. Future work will include the investigation of EOF analysis for SLP and precipitation to examine whether the formation and physical dynamics of these atmospheric amphidromes can be explained.

[35] **Acknowledgments.** We would like to extend our appreciation to Jim and Sara Jones and the anonymous reviewers. Their constructive comments were very valuable in improving the quality of this paper. This study is cosponsored by the Natural Science Foundation of China under projects 40730530, 40675016, and 40706056.

## References

Adler, R. F., et al. (2003), The version-2 global precipitation climatology project (GPCP) monthly precipitation analysis (1979–present), *J. Hydrometeorol.*, *4*, 1147–1167.

Cartwright, D. E. (2001), *Tides: A Scientific History*, Cambridge Univ. Press, New York.

Chen, G. (2004), A 10-yr climatology of oceanic water vapor derived from the TOPEX microwave radiometer, *J. Clim.*, *17*, 2541–2557.

Chen, G., and H. Lin (2005), Impact of El Niño/La Niña on the seasonality of oceanic water vapor: A proposed scheme for determining the ITCZ, *Mon. Weather Rev.*, *133*, 2940–2946.

Chen, G., and G. D. Quartly (2005), Annual amphidromes: A common feature in the ocean?, *IEEE Trans. Geosci. Remote Sens.*, *2*, 423–427.

Gu, D., and S. G. H. Philander (1995), Secular changes of annual and interannual variability in the tropics during the past century, *J. Clim.*, *8*, 864–876.

Hann, J., and R. Süring (1939), *Lehrbuch der Meteorologie*, vol. 1, 5th ed., pp. 259–260, Willibald Keller, Leipzig, Germany.

Hsu, C. P., and J. M. Wallace (1976), The global distribution of the annual and semiannual cycles in sea level pressure, *Mon. Weather Rev.*, *104*, 1597–1601.

Lorenz, E. N. (1951), Seasonal and irregular variations of the Northern Hemisphere sea level profile, *J. Atmos. Sci.*, *8*, 52–59.

Mantua, N. J., S. R. Hare, Y. Zhang, J. M. Wallace, and R. C. Francis (1997), A Pacific decadal climate oscillation with impacts on salmon, *Bull. Am. Meteorol. Soc.*, *78*, 1069–1079.

McPhaden, M. J. (1999), Genesis and evolution of 1997–1998 El Niño, *Science*, *283*, 950–954.

Newman, M., G. P. Compo, and M. A. Alexander (2003), ENSO-forced variability of the Pacific Decadal Oscillation, *J. Clim.*, *16*, 3853–3857.

Philander, S. G. H. (1983), El Niño Southern Oscillation phenomena, *Nature*, *302*, 295–301.

Rasmusson, E., and T. Carpenter (1982), Variations in tropical sea surface temperature and surface wind fields associated with the Southern Oscillation/El Niño, *Mon. Weather Rev.*, *110*, 354–384.

Smith, T. M., and R. W. Reynolds (2004), Reconstruction of monthly mean oceanic sea level pressure based on COADS and station data (1854–1997), *J. Atmos. Ocean. Technol.*, *21*, 1272–1282.

van Loon, H. (1967), The half-yearly oscillations in middle and high southern latitudes and the coreless winter, *J. Atmos. Sci.*, *24*, 472–486.

van Loon, H. (1972), Pressure in the Southern Hemisphere, *Meteor. Monogr.*, *35*, 59–86.

Wang, B., R. Wu, and R. Lukas (2000), Annual adjustment of the thermocline in the tropical Pacific Ocean, *J. Clim.*, *13*, 596–616.

Wang, B., and Q. Ding (2006), Changes in global monsoon precipitation over the past 56 years, *Geophys. Res. Lett.*, *33*, L06711, doi:10.1029/2005GL025347.

Xie, P., and P. A. Arkin (1997), Global precipitation: A 17-year monthly analysis based on gauge observations, satellite estimates, and numerical model outputs, *Bull. Am. Meteorol. Soc.*, *78*, 2539–2558.

Zhang, C., and G. Chen (2007), A global analysis of multi-mode sea surface temperature pattern, *Acta Oceanol. Sin.*, *26*, 12–22.

Zhang, Y., J. M. Wallace, and D. S. Battisti (1997), ENSO-like interdecadal variability: 1900–93, *J. Clim.*, *10*, 1004–1020.

Zhang, C., B. Wang, and G. Chen (2006), Annual sea level amphidromes in the South China Sea revealed by merged altimeter data, *Geophys. Res. Lett.*, *33*, L14606, doi:10.1029/2006GL026493.

G. Chen, Ocean Remote Sensing Institute, Ocean University of China, Qingdao 266003, China.

F. Qiu and C. Zhang, Program in Geospatial Information Sciences, University of Texas at Dallas, Richardson, TX 75083, USA. (zhangcy@utdallas.edu)